JOURNAL OF COMPUTATIONAL PHYSICS **138,** 563–584 (1997)
ARTICLE NO. CP975834

Langevin Representation of Coulomb Collisions in PIC Simulations*

Wallace M. Manheimer, Martin Lampe, and Glenn Joyce

Plasma Physics Division, Naval Research Laboratory, Washington, DC 20375-5346
E-mail: lampe@ppd.nrl.navy.mil

Received October 7, 1996; revised July 3, 1997

An efficient grid-based Langevin formulation is developed for treating electron–electron (e-e) and electron–ion collisions within a particle-in-cell plasma simulation code. The formulation is energy- and momentum-conserving. If the thermal part of the electron velocity distribution is reasonably close to isotropy in any local frame of reference, the basic scattering algorithm is quantitatively accurate for electrons with any value of energy. This is particularly important in calculating the approach to equilibrium of the high-energy tail, or the equilibrium under the competing influences of e-e collisions, inelastic electron–neutral collisions, and end losses through sheaths. If the electron velocity distribution is multi-peaked or very anisotropic, accurate calculations can be performed by representing the electrons as a superposition of several beams. Computational examples are given illustrating both equilibrium energy distribution and approach to equilibrium.

Key Words: Coulomb scattering; electron–electron scattering; Langevin equation; plasma simulation; particle-in-cell simulations.

1. INTRODUCTION

The development of particle-in-cell (PIC) simulation codes [1–3] was originally motivated by work on the physics of high-temperature collisionless plasmas. In much of the early work, measures were taken to reduce the influence of numerical collisions and render the simulation as close to collisionless as possible. However, in recent years much interest has been drawn to plasmas where collisions play a central role, such as the low-temperature partially ionized plasmas used for materials processing. In these plasmas, collisions between charged particles and neutral species

* Research supported by the Office of Naval Research.

0021-9991/97 $25.00

are always important; indeed, the gas chemistry that is central to the processes of interest is often driven by electron–neutral (e-n) collisions. Thus, methodologies have been developed for modeling electron–neutral collisions within PIC codes. The most widely used approach is to append a Monte Carlo (MC) step at which probabilistic scattering occurs between a randomly selected charged particle and a neutral particle. Codes of this type are usually called PIC/MC codes [4–13]. A related technique that has been widely used in neutral gas aerodynamics is called direct simulation Monte Carlo (DSMC) [14]. In most cases, electron–electron (e-e) scattering has not been included in PIC/MC codes.

However, in ''high density'' plasmas which are becoming important in semiconductor processing, such as electron cyclotron resonance (ECR), helicon, and inductively coupled plasmas, electron densities can exceed 10^{12} cm^{-3}, and e-e collision frequencies can exceed those of e-n collisions. Even in cases where pitch-angle scattering is predominantly due to e-n collisions, e-e collisions can be crucial in determining the electron energy distribution function (EEDF). In many types of discharge, the energy input is primarily into the thermal part of the EEDF, and the high-energy tail is populated primarily by energy up-scattering consequent to e-e collisions. Electron–electron collisions always drive the EEDF toward Maxwellian, but there may be a competition with inelastic e-n collisions which deplete the high-energy tail, and in a bounded plasma with escape of high-energy electrons to the walls. The high-energy tail controls atomic excitation, ionization, and to some extent plasma chemistry, and thus determines many of the properties of a plasma that are crucial for processing applications. In addition, sheath potentials are determined by the competition between escape of high-energy electrons to the wall and repopulation of the high-energy tail by collisions. Thus, it is essential that both e-e and e-n collisions be modeled accurately, particularly in the case of high density discharges.

We have recently developed a 2-D axisymmetric PIC/MC model of an ECR discharge with strongly magnetized electrons [15]. The unique feature of our model is that both electrons and ions are represented by particles, but the electrostatic field is determined from the requirement of quasineutrality, rather than by solving Poisson's equation. Therefore, plasma oscillations are absent from the model, and it is possible to use time steps many orders of magnitude longer than the electron plasma period, as well as spatial gridding much coarser than the Debye length λ_D. In the model, elastic, inelastic, and ionizing e-n collisions are handled with a Monte Carlo collision scheme. In this paper, we describe the formulation which we have developed to include electron–electron and electron–ion collisions. We believe it is suitable for use in a wide variety of simulation applications.

In DSMC simulations of low-density neutral gases, collisions are modeled by picking out nearby pairs of particles, at regular intervals, and allowing various types of collisions to occur between them. The determination of which type of collision occurs (e.g., elastic, excitation, ionization, etc.) and the value of the scattering angle depend on the choice of random numbers, with probabilities determined by the relevant cross sections. In PIC/MC simulations of plasmas, collisions between charged and neutral particles are treated in a somewhat similar way, but usually

the grid is used as an intermediary in the collision process, i.e., the density of a particular neutral species is laid down on the grid, and then the probability of an electron colliding with that species is proportional to the density. The most straightforward way to represent e-e collisions in a PIC code would be to use the DSMC procedure, i.e., at appropriate time intervals, to pick out a number of pairs of electrons and collide them with the statistics appropriate to individual electron–electron collisions. The problem with this approach is that e-e collisions occur predominantly at long range, so that they are actually a succession of very many small angle scatterings. In order to represent individual collisions with any degree of accuracy, it would be necessary to use an extremely small time step. In fact, even at a given instant of time, an electron will typically be scattering off many other electrons simultaneously. Thus it is numerically inefficient, and really inappropriate physically, to treat e-e scattering as a sequence of MC collisions. Weng and Kushner [18] used an approach rather more in the spirit of plasma PIC/MC, where electrons collided off electron density/energy distributions laid down on the grid, with statistics chosen as a rough approximation to the Coulomb cross section for individual e-e collisions. Although this approach has some numerical advantages over the DSMC approach, it still suffers from the requirement of an extremely small time step to resolve the time between individual collisions.

An alternative approach which has been emphasized in the analytical development of plasma kinetic theory is to represent Coulomb scattering through a Fokker–Planck equation [19–21]. Direct numerical solutions of the Fokker–Planck equation are often performed [22, 23], but there is no obvious way to combine this procedure with a PIC simulation. However, it is possible to construct a Langevin equation (comprising a deterministic friction and a random diffusive scattering) which is entirely equivalent to any given Fokker–Planck equation [24]. In the context of a PIC simulation, the dynamical friction and stochastic diffusion coefficients for the Langevin equation can be represented as velocity-dependent grid quantities, which are simply added to the macroscopic electric and magnetic forces acting on the electrons. Thus, e-e scattering is in effect represented as a scattering of a single electron off the grid, rather than as a pairwise process.

A grid-based Langevin formalism for e-e scattering has recently been developed by Jones *et al.* [25]. In this paper, a key simplification is made, which eases the implementation of the scheme. This is the representation of e-e scattering as an isotropic scattering process characterized by a velocity-independent collision frequency ν. This leads to a dynamical friction $\mathbf{F}_d$ of the form

$$\mathbf{F}_d = -m\nu\mathbf{v}, \tag{1a}$$

and a scalar velocity-independent velocity-space diffusion coefficient D,

$$D = 2\nu T/m, \tag{1b}$$

where $\mathbf{v}$ is the velocity of the test particle, and T is the electron temperature. These coefficients $\mathbf{F}_d$ and D are consistent with each other, and therefore the

Langevin equation conserves momentum and energy (to first order in the time step), and correctly drives the EEDF toward a Maxwellian distribution with zero mean velocity and temperature T. Furthermore, Jones *et al.* [25] use the Spitzer value of ν, which is an appropriate average over an assumed Maxwellian velocity distribution of test and field electrons. For many applications, these properties may be sufficient. However, the Coulomb scattering process is in fact highly anisotropic. Nearly all scattering events are very weak; as a result the parallel component D_{33} of the diffusion tensor is much smaller than the perpendicular component D_{11}. Even more significantly, the scattering rate is strongly velocity dependent, with ν falling off as $\mathbf{v}^{-3}$ for superthermal electrons. Consequently, the averaged coefficients $\mathbf{F}_d$ can be over an order of magnitude too large for superthermal electrons. The time scale for populating the tail of the EEDF is very much understated by these equations, and if there is competition between e-e collisions and inelastic e-n collisions, the use of Eqs. (1) can give a very inaccurate picture of the EEDF in steady state.

In this paper, we build on the work of Jones *et al.* [25] to construct a Langevin scattering formalism which accurately represents the multiple small-angle Coulomb scattering process, with velocity-dependent friction and diffusion coefficients derived from the actual electron distribution. The derivation of these coefficients is reviewed in Section 2. One key approximation is made which enormously simplifies the formulation and reduces the size of the data sets needed: in calculating the dynamical friction $\mathbf{F}_d$ and the diffusion tensor $\mathbf{D}$, it is assumed that the velocity distribution function of scatterer electrons is isotropic in its mean frame of reference, i.e., is a function only of $|\mathbf{v} - \mathbf{u}_e|$, where $\mathbf{u}_e$ is the local electron fluid velocity. The range of validity of this approximation is discussed in the Appendix. Roughly speaking, it is quantitatively accurate at least over the range where the aspect ratio of the distribution is less than 2:1. For more extreme anisotropy, e.g., multiple beams, accuracy can be restored by representing the scatterers as several isotropic distributions displaced from each other in velocity space.

In Section 3 we consider the application of the formalism to a magnetized-electron plasma such as our ECR discharge plasma. In order to reduce calculation time, data complexity and statistical fluctuations, the normalized EEDF used to calculate $\mathbf{F}_d$ and $\mathbf{D}$ is averaged over a field line (but the actual electron density at each grid cell is used). The basic Langevin formulation is energy and momentum conserving, but some of the approximations, finite time steps, and statistical fluctuations can introduce minor deviations from conservation. In Sections 2 and 4 we show how to restore exact conservation in an efficient way. In Section 5 we discuss the extension of the Langevin scattering formalism to electron–ion scattering, which is in fact very much simpler than e-e scattering. In Section 6, we show the results of several computational exercises, which demonstrate the way in which e-e collisions drive the electron distribution first toward isotropy, and then (in the absence of other collisional processes) toward a Maxwellian. We also show, using a simplified model of an argon plasma, how the competition between e-e collisions and inelastic e-n collisions determines the high-energy tail of the EEDF. In Section 7 the results are summarized.

2. GENERAL FORMULATION

A. *Review of the Derivation of the Fokker–Planck Equation for Coulomb Scattering*

The formulation of the Langevin equation for the electrons starts with the Boltzmann collision integral for electron–electron collisions

$$\left.\frac{\partial f(\mathbf{v},t)}{\partial t}\right|_{ee} = n\int d^3\,\tilde{\mathbf{v}}\, g\,\frac{d\sigma}{d\Omega}\,[f(\mathbf{v}')f(\tilde{\mathbf{v}}') - f(\mathbf{v})f(\tilde{\mathbf{v}})], \tag{2}$$

where the tilde indicates the field electron with which the electron of interest is colliding, the prime refers to the value of a quantity after a collision, and unprimed denotes the value before the collision, $\mathbf{g} \equiv \mathbf{v} - \tilde{\mathbf{v}}$ is the relative velocity, n is the electron number density, and the electron distribution functions are normalized to unity. The Coulomb scattering cross section is [21]

$$\frac{d\sigma}{d\Omega} = \frac{e^4}{m^2 g^4 \sin^4(\theta/2)}, \tag{3}$$

where θ is the scattering angle in the center of mass frame. For electron–electron scattering, θ is related to the impact parameter b by

$$\theta = 2\tan^{-1}\left(\frac{2e^2}{mg^2 b}\right). \tag{4}$$

The relative velocity after the scattering is

$$\mathbf{g}' = \mathbf{g} + \Delta\mathbf{g} \tag{5}$$

and of course, the scattering is a rotation in the center of mass frame, so $g' = g$. If the 3-coordinate is taken parallel to $\mathbf{g}$, and the 1,2 coordinates perpendicular to $\mathbf{g}$, then

$$\Delta\mathbf{g} = \mathbf{g}\{\sin\theta\cos\phi, \sin\theta\sin\phi, -2\sin^2(\theta/2)\} \tag{6}$$

and

$$\mathbf{v}_i' = \mathbf{v}_i + \Delta\mathbf{g}/2, \qquad \mathbf{v}_j' = \mathbf{v}_j - \Delta\mathbf{g}/2. \tag{7}$$

Because of the $\sin^{-4}(\theta/2)$ dependence of the scattering cross section for the Coulomb potential, the collisions are dominated by multiple small-angle scattering. In fact, when integrating Eq. (2) over θ, the result diverges logarithmically as the lower limit of integration θ_m approaches zero. This divergence is resolved by assuming that the Coulomb force is shielded over a distance of order the Debye length, and therefore setting the minimum scattering angle θ_m equal to

$$\theta_m = 2\tan^{-1}\left(\frac{2e^2}{mg^2\lambda_D}\right). \tag{8}$$

The terms $f(\mathbf{v}')$ and $f(\tilde{\mathbf{v}}')$ in the integrand can then be expanded in powers of $\Delta\mathbf{g}$. It is not difficult to show that the only terms which suffer the divergence as $\ln\theta_m$ are the terms involving the first and second derivatives of $f(\mathbf{v})$. These are therefore the dominant terms, and it is appropriate to neglect higher order. One further approximation is made: in the specification of θ_m, Eq. (8), the relative velocity g of the pair of colliding electrons is replaced by the root-mean-square average electron velocity v_e. Since the dependence on θ_m is very weak (logarithmic), the results are insensitive to this approximation, which greatly simplifies the formalism. This leads to the standard expression [19–21]

$$\left.\frac{\partial f}{\partial t}\right|_{ee} = -\frac{\partial}{\partial\mathbf{v}}\cdot\mathbf{F}_{\mathrm{d}}(\mathbf{v})f(\mathbf{v}) + \frac{1}{2}\frac{\partial^2}{\partial\mathbf{v}\partial\mathbf{v}}:f(\mathbf{v})f(\mathbf{v}), \tag{9}$$

where

$$\mathbf{F}_{\mathrm{d}}(\mathbf{v}) = \frac{4\pi ne^4}{m^2}\lambda\frac{\partial H}{\partial\mathbf{v}}, \tag{10a}$$

$$\mathbf{D}(\mathbf{v}) = \frac{4\pi ne^4}{m^2}\lambda\frac{\partial^2 G}{\partial\mathbf{v}\partial\mathbf{v}}, \tag{10b}$$

$$\lambda = \ln\left(\frac{1}{2}\csc\theta_m\right), \tag{11a}$$

$$\theta_m = 2\tan^{-1}\left(\frac{2e^2}{mv_e^2\lambda_D}\right), \tag{11b}$$

$$H(\mathbf{v}) = 2\int\mathbf{d}^3\tilde{\mathbf{v}}\frac{f(\tilde{\mathbf{v}})}{|\mathbf{v}-\tilde{\mathbf{v}}|}, \tag{12a}$$

$$G(\mathbf{v}) = \int d^3\tilde{\mathbf{v}}f(\tilde{\mathbf{v}})|\mathbf{v}-\tilde{\mathbf{v}}|. \tag{12b}$$

This then defines the Fokker–Planck equation for electron–electron scattering. The coefficients $G(\mathbf{v})$ and $H(\mathbf{v})$, which govern the diffusion and dynamic friction, are scalar functions of the vector velocity $\mathbf{v}$. Since the Fokker–Planck equation is the lowest order expansion of the Boltzmann collision integral in powers of λ^{-1}, it retains the important characteristics of the Boltzmann collision integral. These include the H theorem (i.e., it drives the electron distribution function to a Maxwellian), as well as conservation of energy and momentum.

B. *Isotropic Scatterer Approximation*

In typical applications to PIC codes, it would be completely impractical (in terms of numbers of particles, computation time, and statistical fluctuations) to actually compute the coefficients $H(\mathbf{v})$ and $G(\mathbf{v})$ as multiple integrals, and then perform

numerical differentiations. However, the Fokker–Planck equation can be reduced to a much more tractable form by assuming in Eqs. (12) that the distribution function $f(\tilde{\mathbf{v}})$ of scatterer electrons is a function of only the magnitude of the velocity, in the reference frame in which the electron fluid velocity $\mathbf{u}_e$ is zero. If this is not exactly true, then we replace $f(\tilde{\mathbf{v}})$ with

$$\bar{f}(|\tilde{\mathbf{v}} - \mathbf{u}_e|) \equiv \frac{1}{4\pi} \int_0^\pi d\theta \int_0^{2\pi} d\phi f(\mathbf{v}), \tag{13}$$

where we have averaged over the polar angles in a spherical coordinate system centered on $\mathbf{u}_e$. In collisional systems, this is normally a reasonably good approximation, since all electron collisions tend to isotropize the electron distribution function. The thermal part of the electron distribution isotropizes particularly rapidly, and e-e scattering of *any* electron (even a fast one) is normally dominated by scattering off thermal electrons. In the Appendix, we consider the question of the limits of validity of the approximation in very anisotropic situations. Our conclusion is that the approximation retains quantitative accuracy at least in situations where the distribution $f(\mathbf{v} - \mathbf{u}_e)$ is single-peaked and isotropic to within a 2:1 temperature ratio. For more extreme anisotropy, e.g., for multiple beams, it is always possible to restore accuracy by representing the scatterers as the superposition of several isotropic distributions displaced from each other in velocity space.

We emphasize that in the Fokker–Planck equation (9), it is *not* necessary to assume that the test particle distribution $f(\mathbf{v})$ is isotropic. It is often reasonably accurate to follow the evolution of a mildly anisotropic test particle distribution while assuming that the scattering is off an isotropic distribution of field particles. However, this approximation does interfere with the exact conservation of momentum and energy which is a property of Eq. (9). In Section 4 we discuss methods to ensure conservation.

When the assumption of isotropic scatterers is made, the integrals over the polar and azimuthal angles in velocity space can be done in closed forms, and Eqs. (12) reduce to

$$H(\mathbf{v}) = \frac{8\pi}{v} \int_0^v d\tilde{v}\tilde{v}^2 f(\tilde{v}) + 8\pi \int_v^\infty d\tilde{v}\tilde{v} f(\tilde{v}), \tag{14a}$$

$$G(v) = \frac{4\pi}{3} \left[\int_0^v d\tilde{v}\tilde{v}^2 \frac{3v^2 + \tilde{v}^2}{v} f(v) + \int_v^\infty d\tilde{v}\tilde{v}(v^2 + 3\tilde{v}^2) f(\tilde{v}) \right]. \tag{14b}$$

The velocity derivatives in Eqs. (10) can then be calculated analytically from Eqs. (14), which greatly reduces noise in the simulation. We find $\mathbf{F}_d(\mathbf{v}) = \mathbf{F}_d(v)(\mathbf{v}/v)$, with

$$F_d(v) = \frac{4\pi n e^4}{m^2} \lambda \frac{dH}{dv} = -\frac{32\pi^2 n e^4}{m^2 v^2} \lambda \int_0^v d\tilde{v}\tilde{v}^2 f(\tilde{v}). \tag{15a}$$

Since G is a scalar function of the scalar variable v, the tensor $\partial^2 G/\partial\mathbf{v}\partial\mathbf{v}$ is diagonal in a coordinate system where the 3-component is parallel to $\mathbf{v}$. The only non-zero components of the tensor $\mathbf{D}$ are

$$D_{33}(v) = \frac{4\pi ne^4}{m^2}\lambda\frac{\partial^2 G}{\partial v_3 \partial v_3} = \frac{4\pi ne^4}{m^2}\lambda\frac{d^2G}{dv^2}$$

$$= \frac{32\pi^2 ne^4}{3m^2}\lambda\left[\frac{1}{v^3}\int_0^v d\tilde{v}\tilde{v}^4 f(\tilde{v}) + \int_v^\infty d\tilde{v}\tilde{v} f(\tilde{v})\right], \tag{15b}$$

$$D_{11}(v) = D_{22}(v) = \frac{4\pi ne^4}{m^2}\lambda\frac{\partial^2 G}{\partial v_1 \partial v_1} = \frac{4\pi ne^4}{m^2}\lambda\frac{1}{v}\frac{dG}{dv}$$

$$= \frac{16\pi^2 ne^4}{3m^2}\lambda\left[\frac{1}{v^3}\int_0^v d\tilde{v}\tilde{v}^2(3v^2 - \tilde{v}^2) f(\tilde{v}) + 2\int_v^\infty d\tilde{v}\tilde{v} f(\tilde{v})\right]. \tag{15c}$$

It will be noted that $F_d(v)/v$, $D_{33}(v)$, and $D_{11}(v)$ are all monotonically decreasing functions of v, with the first two decreasing as v^{-3} for high-energy electrons and the latter as v^{-1}. As a result, the approach to equilibrium, and the continuing effect of e-e collisions, are much weaker at high energies. To illustrate this, the three coefficients are plotted in Fig. 1 as a function of $v/\sqrt{2}v_e$, for the case of a Maxwellian distribution $f(v) = (m/2\pi T)^{3/2}\exp(-v^2/2v_e^2)$, with $v_e = (T/m)^{1/2}$ the thermal velocity. For comparison, the velocity-independent average transport coefficients used by Jones *et al.* [25] are plotted as dashed lines. It is apparent that this model, or any model based on an assumed energy-independent collision frequency, significantly overestimates the effect of e-e collisions for superthermal electrons.

Another type of approximation is usually necessary, due to the fact that the number of particles in a simulation will normally be too small to calculate the integrals in Eqs. (15) at every grid point, and the time involved would be inordinate. Therefore, it is necessary to perform some type of spatial or temporal averaging in this step. In Section 3, we show exactly how we choose to do this in our magnetized-electron simulation.

C. *Formulation of the Langevin Equation*

In order to utilize this formulation in a PIC code, it is necessary to go from the Fokker–Planck equation to the Langevin equation. To first order accuracy in Δt, the Langevin equation in the form

$$\Delta\mathbf{v} = \mathbf{F}_d\Delta t + \mathbf{Q}, \tag{16}$$

is equivalent to the Fokker–Planck equation (9). Here $\Delta\mathbf{v}$ is the change in a particle's velocity, due to e-e scattering, during a finite time step Δt, F_d is the dynamical friction, and $\mathbf{Q}$ is a random velocity vector chosen from the distribution

$$\phi(\mathbf{Q}) = \frac{1}{(2\pi\,\Delta t)^{3/2}D_{11}D_{33}^{1/2}}\exp\left(-\frac{Q_3^2}{2D_{33}\,\Delta t} - \frac{Q_1^2 + Q_2^2}{2D_{11}\,\Delta t}\right). \tag{17}$$

However, using Eqs. (15)–(17) and taking averages over the stochastic variable $\mathbf{Q}$, one can easily show that there is an error of order $(\Delta t)^2$, always positive, in the total electron energy ε after the collision step, i.e.,

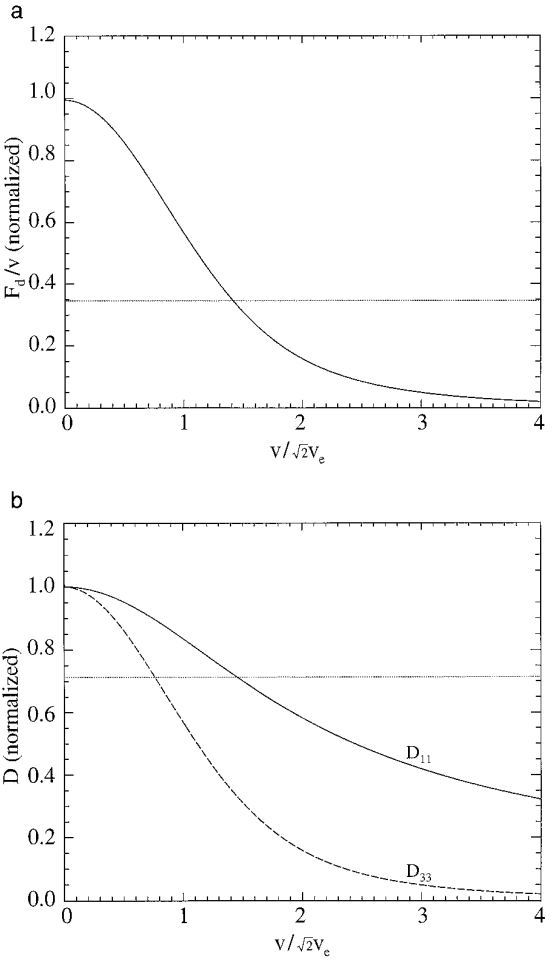

FIG. 1. (a) $F_d(v)/v$ from Eq. (15a) for a Maxwellian distribution. (b) $D_{11}(v)$ and $D_{33}(v)$ from Eqs. (15b,c). The dashed lines are the velocity-independent average values used in [23].

$$\langle \varepsilon' \rangle - \varepsilon = 2\pi m (\Delta t)^2 \int_0^\infty dv v^2 F_d^2 f(v). \tag{18}$$

Exact energy conservation (as an ensemble average over the stochastic variable **Q**) can be restored by simply adding a correction $\delta F(v)$ to $F_d(v)$, specified by the equation

$$\left(1 + \frac{F_d \Delta t}{v}\right) \delta F + \frac{\Delta t}{2v} (\delta F)^2 = -\frac{\Delta t}{2v} F_d^2. \tag{19}$$

For most purposes, it is more than adequate to ensure that the Langevin equation conserves energy to second order in Δt, which will hold if $\delta F(v)$ is given by the much simpler approximate form of Eq. (19),

$$\delta F(v) = -\frac{\Delta t}{2v} F_{\mathrm{d}}^2(v). \tag{20}$$

We note in passing a surprising property of Eq. (15a): for a test electron with speed v, scattering off electrons with speed $\tilde{v} \geq v$ does not contribute to the friction coefficient $\mathbf{F}_{\mathrm{d}}(v)$. This is a peculiarity of Coulomb scattering off an isotropic distribution of scatterers [26, 27]. As a result, the friction is very small for electrons with velocity much less than the thermal velocity v_{e}, and if the EEDF happens to be hollow, with $v \geq v_{\min}$ for all electrons, then an electron with $v = v_{\min}$ will feel no friction at all. At first sight, it seems paradoxical that such electrons will not be driven toward a distribution centered about the mean electron velocity $\mathbf{u}_{\mathrm{e}}$. However, what actually happens is that a low-velocity electron will, on the average, diffuse up toward speed v_{e} (the diffusion coefficients have contributions from scattering off electrons with $\tilde{v} \geq v$, and do not go to zero for small v), and then feel a strong friction that tends on the average to center it about $\mathbf{u}_{\mathrm{e}}$.

3. APPLICATION TO A MAGNETIZED PLASMA

A. *Langevin Scattering Formulation for Magnetized Electrons*

This electron–electron scattering model was developed primarily for use in our recently developed 2D-3v (axisymmetric) simulation model of ECR processing plasmas [15–17]. In this code, both the electrons and ions are represented as simulation particles, subject to a strong external magnetic field, self-consistently determined electrostatic fields, and collisions. The ions are not typically strongly magnetized; hence their trajectories are followed in full detail in two spatial and three velocity coordinates. However, the electrons are strongly magnetized, and can be regarded as firmly attached to a given magnetic field line. This is a good approximation as long as the electron Larmor radius is very small compared to any macroscopic length scale, and the electrons escape to the walls before they undergo significant collisional diffusion across field lines. (Because of the axisymmetry, all drifts are azimuthal, and thus do not take the electrons across field lines in the r-z plane of the simulation.) Thus, we use the actual field lines as one set of elements for a curvilinear grid, allowing us to specify the position of an electron by the field line number to which it is permanently attached, and a single axial coordinate z giving its location on the field line. In velocity space, the code follows the parallel velocity $v_{\parallel}$ of each electron, and the magnitude of the perpendicular velocity $v_{\perp}$, but there is no need to follow the phase of the perpendicular motion. In practice, we follow the magnetic moment $\mu \equiv m v_{\perp}^2/2|\mathbf{B}|$, which is constant during the interval between collisions, rather than propagating $v_{\perp}$ itself. The unique feature of our simulation is that Poisson's equation is not used, but rather the electric field is obtained from the quasineutrality, much like the procedure that is used in fluid simulations. This allows the simulation to avoid inverse plasma frequency time scales and Debye length scales. For both electrons and ions, the relevant length scale is the macroscopic length scale, and the minimum time scale is this length scale divided by the electron thermal velocity. This simulation scheme speeds up the calculation by

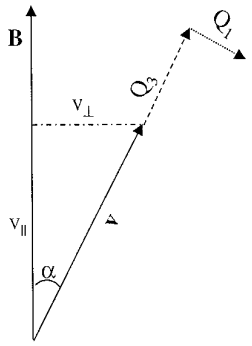

FIG. 2. Geometry for the transformation from coordinate 3 (parallel to the velocity **v** before scattering), 1 (normal to **v** but in the **B-v** plane), 2 (normal to both **B** and **v**) to coordinates $\parallel$ (parallel to **B**) and $\perp$ (normal to **B**).

several orders of magnitude for the usual ECR reactor as compared to a standard particle in cell code with the electrostatic field calculated from Poisson's equation. The details of the simulation scheme and some results are given elsewhere [15–17].

In applying the e-e scattering formalism to this type of guiding center electron model, it is necessary only to specify the value of $v_\parallel'$ and $v_\perp'$ after the collision, given $v_\parallel$ and $v_\perp$ before the collision. To transform the Langevin scattering results to these variables, it is convenient to use a coordinate system with the 3-coordinate parallel to **v**, the electron's velocity before collision, the 1-coordinate normal to **v** but in the **B-v** plane, and the 2-coordinate normal to both **B** and **v**, as shown in Fig. 2. Let α be the angle between **B** and **v**, so that $\tan\alpha = v_\perp/v_\parallel$. After scattering, the new vector $\mathbf{v}'$ is given by

$$v_1' = Q_1, \tag{21a}$$

$$v_2' = Q_2, \tag{21b}$$

$$v_3' = v + F_d \Delta t + Q_3. \tag{21c}$$

Transforming back to $v_\parallel'$ and $v_\perp'$, we find from Fig. 1 that

$$v_\parallel' = v_3' \cos\alpha - v_1' \sin\alpha = (v + F_d\,\Delta t + Q_3)\cos\alpha - Q_1 \sin\alpha. \tag{22a}$$

$$v_\perp'^2 = (v_3' \sin\alpha + v_1' \sin\alpha)^2 + v_2'^2 = [(v + F_d\,\Delta t + Q_3)\sin\alpha + Q_1 \cos\alpha]^2 + Q_2^2. \tag{22b}$$

Equations (22), together with Eqs. (15)–(17), give the basic Langevin formulation for the e-e scattering in a magnetized system.

B. *Data Structure and Numerical Considerations*

By assuming that the distribution of scatterers is isotropic, we have reduced the scattering coefficients $F_d(v)$, $D_{11}(v)$, and $D_{33}(v)$ to grid-dependent quantities that also depend on the magnitude v of the test electron velocity. However, statistical

fluctuations incident to the finite number of simulation particles would make it virtually impossible to actually compute these velocity-dependent coefficients by performing the velocity integrals of Eq. (15) at every grid point. (It would also be inordinately time consuming.) For example, in a two-dimensional PIC simulation with a 100×100 grid, even with a million particles there are only 100 particles per cell, leading to fluctuations at least on the order of 10% (and even worse for v-dependent quantities). Clearly, it is necessary to perform some spatial and/or temporal averaging, which should be specified in accordance with the circumstances under consideration. For example, in our magnetized-electron code, we construct the *normalized* velocity distribution $f_j(v)$ for all of the electrons on field line j, and use this $f_j(v)$ to calculate the velocity integrals in Eqs. (15). However, the density n used in Eq. (15) is taken to be the local electron density on the grid. This is a reasonable approximation in our case, since the electron fluid velocity $\mathbf{u}_e$ is always small compared to the thermal velocity $\mathbf{v}_e$ (and therefore can be regarded as essentially uniform), and most electrons sample an entire field line on the fast time scale L/v_e, where L is the length of the field line. [Some electrons can be trapped for a while in potential minima; if it is important to consider this in the scattering formulation, $f(v)$ can be constructed over some smaller region, rather than the entire field line.] It is also a very efficient procedure, since the integral quantities in (15) can simply be accumulated at the same time that the particle densities are laid down on the grid.

In the next section, we show how to build exact energy and momentum conservation into the scattering formalism. If the conservative form (23) or (24) is used, the only limits imposed on the scattering time step Δt are those necessary to ensure accuracy. Thus, Δt should be no more than a fraction of the e-e collisional relaxation time. In many cases, there will be stronger constraints imposed by other aspects of the simulation. For example, if e-e scattering is competing with inelastic electron–neutral scattering, then Δt should be no larger than the characteristic time for the latter process. In a bounded plasma, sheath potentials may be determined by competition between escape of high-energy electrons through the sheath, and replenishment of high-energy electrons via e-e collisions. Then Δt must be no larger than the time step used for electron escape. In other cases, the limit on Δt may arise from the characteristic time for electrons to transport spatially from one region to another.

4. ENERGY AND MOMENTUM CONSERVATION

The Fokker–Planck equation (9), with coefficients from Eqs. (10)–(12), exactly conserves momentum and energy. However, the numerical implementation of e-e scattering, as described in Sections 2 and 3, may suffer small deviations from momentum and energy conservation. Errors in energy conservation are particularly troublesome, since Lemons *et al.* [28] have shown that they can lead to systematic (non-random) drifts in total energy that can become substantial over long times. These types of effects could lead to significant errors in EEDF, and therefore in ionization fraction, chemical make-up, and other such properties of the plasma.

Momentum conservation errors may also be of concern, if they interfere with the calculation of electric currents to sufficient accuracy.

Momentum and energy non-conservation can occur for two reasons. First, if the electron velocity distribution $f(\mathbf{v})$ is not exactly isotropic, the assumption of an isotropic distribution $f(v)$ for the scatterers is inconsistent with the conservation laws, even if the mean electron velocity $\mathbf{u}_e$ is zero. Obviously, the situation will be worse if $\mathbf{u}_e$ is non-zero and the isotropic distribution $f(v)$ is prepared in a frame of reference other than that of $\mathbf{u}_e$. In Section 3, we have chosen to calculate $f(v)$ in the lab frame for all the electrons on a given field line, so if $\mathbf{u}_e$ is non-uniform along the field line, the scattering formalism clearly will not conserve electron momentum locally. Second, the diffusion part of the Langevin equation involves the choice of random velocity increments $\mathbf{Q}$. On the average, these increments will conserve energy and momentum, but given the finite number of simulation particles N at any grid cell, errors of the order of $\sqrt{N}$ can always occur.

Fortunately, these non-conservation effects are small, particularly if $u_e \ll v_e$, as is the case in our ECR plasma simulations and many other typical situations. It is then particularly easy to make corrections that adequately restore the conservation laws. In general, one can restore momentum and energy conservation locally by using a renormalization procedure described by Lemons *et al.* [28]. We take note of the electron fluid velocity $\mathbf{u}_{e\parallel}(z)$ and the electron temperature $T_e(z)$ on field line j before the e-e scattering step, and the values $\mathbf{u}'_{e\parallel}(z)$ and $T'_e(z)$ after scattering. In general, they will be slightly different. We then reset the velocity $\mathbf{v}'_n$ of electron n located at z, according to the formula

$$\bar{\mathbf{v}}'_n = \mathbf{u}_e + \sqrt{\frac{T_e}{T'_e}}(\mathbf{v}'_n - \mathbf{u}'_e). \tag{23}$$

In practice, we find that Eq. (23) is overkill. Small random errors in electron momentum conservation during e-e collisions are usually unimportant, since collisions of electrons with neutrals and/or ions control the electron current. Furthermore, it is usually sufficient to ensure energy conservation globally over some large area, in our case over a field line, since the velocity integrals in Eq. (15) are performed as an average over a field line. Thus we use the very simple velocity renormalization

$$\bar{\mathbf{v}}'_n = \sqrt{\frac{W_j}{W'_j}}\,\mathbf{v}'_n, \tag{24}$$

where W_j is the total kinetic energy of all the electrons on field line j before the e-e collision step, and W'_j is the same quantity after the collision step.

5. ELECTRON–ION SCATTERING

The Fokker–Planck equation for electron–ion (e-i) scattering is derived in exactly the same way as Eqs. (9)–(12). The only difference in the results is that Eqs. (12) are replaced with

$$H(v) = Z_i^2 \frac{m_e + m_i}{m_i} \int d^3\tilde{\mathbf{v}} \frac{f_i(\tilde{\mathbf{v}})}{|\mathbf{v} - \tilde{\mathbf{v}}|}, \tag{25a}$$

$$G(\mathbf{v}) = Z_i^2 \int d^3\tilde{\mathbf{v}} f_i(\tilde{\mathbf{v}}) |\mathbf{v} - \tilde{\mathbf{v}}|, \tag{25b}$$

where $Z_i e$ is the ion charge and $f_i(\mathbf{v})$ is the ion velocity distribution.

The rate of energy exchange between electrons and ions is down by order m_e/m_i, which makes it negligible for many purposes. If we neglect energy exchange, and treat e-i scattering as essentially just pitch-angle scattering of the electrons off infinitely massive ions, then the formalism becomes particularly simple. It is then appropriate to approximate the ion velocities, which are always small compared to v_e, as zero, so that Eqs. (25) reduce simply to

$$H = \frac{Z_i^2}{v}, \tag{26a}$$

$$G = Z_i^2 v. \tag{26b}$$

According to Eqs. (14), the dynamical friction coefficient is

$$F_d = -\frac{4\pi n e^2 Z_i^2}{m^2 v^2} \lambda, \tag{27a}$$

and the diffusion coefficients are

$$D_{33}(v) = 0, \tag{27b}$$

$$D_{11}(v) = D_{22}(v) = \frac{4\pi n e^4 Z_i^2}{m^2 v} \lambda. \tag{27c}$$

For scattering of electrons off infinitely massive ions, momentum conservation is not a consideration. Electron energy should be conserved exactly in every collision, so the simplest procedure is to not use the dynamical friction from Eq. (27a), but simply to specify Δv_3 so as to ensure exact energy conservation:

$$(v + \Delta v_3)^2 + Q_1^2 + Q_2^2 = v^2, \tag{28}$$

where Q_1 and Q_2 are the stochastic increments to the velocity components normal to $\mathbf{v}$, chosen from the distribution (17). If we neglect second order in Q_1/v and Q_2/v, Eq. (28) becomes simply

$$\Delta v_3 = \frac{Q_1^2 + Q_2^2}{2v}, \tag{29}$$

and in the case of magnetized electrons, the electron velocity components parallel and perpendicular to $\mathbf{B}$, from Eqs. (28), become

$$v_\parallel' = \left(v - \frac{Q_1^2 + Q_2^2}{2v}\right)\cos\alpha - Q_1 \sin\alpha, \tag{30a}$$

$$v_\perp'^2 = \left[\left(v - \frac{Q_1^2 + Q_2^2}{2v}\right)\sin\alpha + Q_1\cos\alpha\right]^2 + Q_2^2. \tag{30b}$$

If it is important to calculate energy transfer between the electrons and ions, it is easy to modify the formalism to include this effect.

6. COMPUTATIONAL EXAMPLES

In this section, we present some simple computational examples as test cases for our formulation of e-e scattering. We consider a 1-D system with periodic boundary conditions and spatially uniform initial conditions (e.g., density, distribution function). Since every cell is identical, and there are no end losses such as would occur in a bounded plasma, this is really a point problem from a fundamental point of view. Nonetheless, it is useful in the context of our 2D ECR plasma code to think of it as a single magnetic field line, with uniform magnetic field, since this is the way the data structures and statistical properties of the simulation are organized. The system length is 35 cm and the cell size is $\Delta z = 1$ cm. We use 15,000 macroparticles to represent the electrons. The electrons are scattered according to Eqs. (15)–(18) at intervals $\Delta t = 8 \times 10^{-9}$ sec.

A. *Approach to Equilibrium*

Here we consider the evolution of the electron distribution from an anisotropic and non-Maxwellian initial condition, with e-e scattering the only physical process represented in the simulation. The initial distribution is a flat-topped cylinder in velocity space,

$$f(v_\parallel, v_\perp, t = 0) = \frac{1}{2\pi v_{\parallel 0} v_{\perp 0}^2}\,\Theta(v_{\parallel 0} - |v_\parallel|)\Theta(v_{\perp 0} - v_\perp), \tag{31}$$

where $\Theta(v)$ is the step function, $\frac{1}{2}mv_{\parallel 0}^2 = 2$ eV and $\frac{1}{2}mv_{\perp 0}^2 = 4$ eV, so that the parallel temperature (defined as the mean $\langle mv_\parallel^2\rangle$) is $T_\parallel = 1.33$ eV and the perpendicular temperature (defined as the mean $\langle \frac{1}{2}mv_\perp^2\rangle$ since there are two degrees of freedom) is $T_\perp = 2$ eV. The plasma density is 10^{12} cm^{-3}.

We recall that the diffusion coefficients of Eqs. (15) decrease rapidly with particle speed v, so that one expects the approach to equilibrium to proceed rapidly for electrons in the low-energy (thermal) range, and more slowly in the high-energy tail. Figure 3 shows plots of the reduced electron distribution functions $f(v_\parallel) \equiv \int_0^\infty dv_\perp\, 2\pi v_\perp f(\mathbf{v})$ and $f(v_\perp) \equiv \int_{-\infty}^{\infty} dv_\parallel f(\mathbf{v})$ at four different times. To exhibit Maxwellians as straight lines, the abscissa in these plots is chosen to be $\varepsilon_\parallel \equiv \frac{1}{2}m_e v_\parallel^2$ or $\varepsilon_\perp \equiv \frac{1}{2}m_e v_\perp^2$. In Fig. 3b, at the early time $t = 1 \times 10^{-8}$ sec, the distribution functions have become rounded but are still anisotropic and non-Maxwellian. Figure 3c shows the distribution functions at $t = 7 \times 10^{-8}$ sec. By this time, the distribution is isotropic

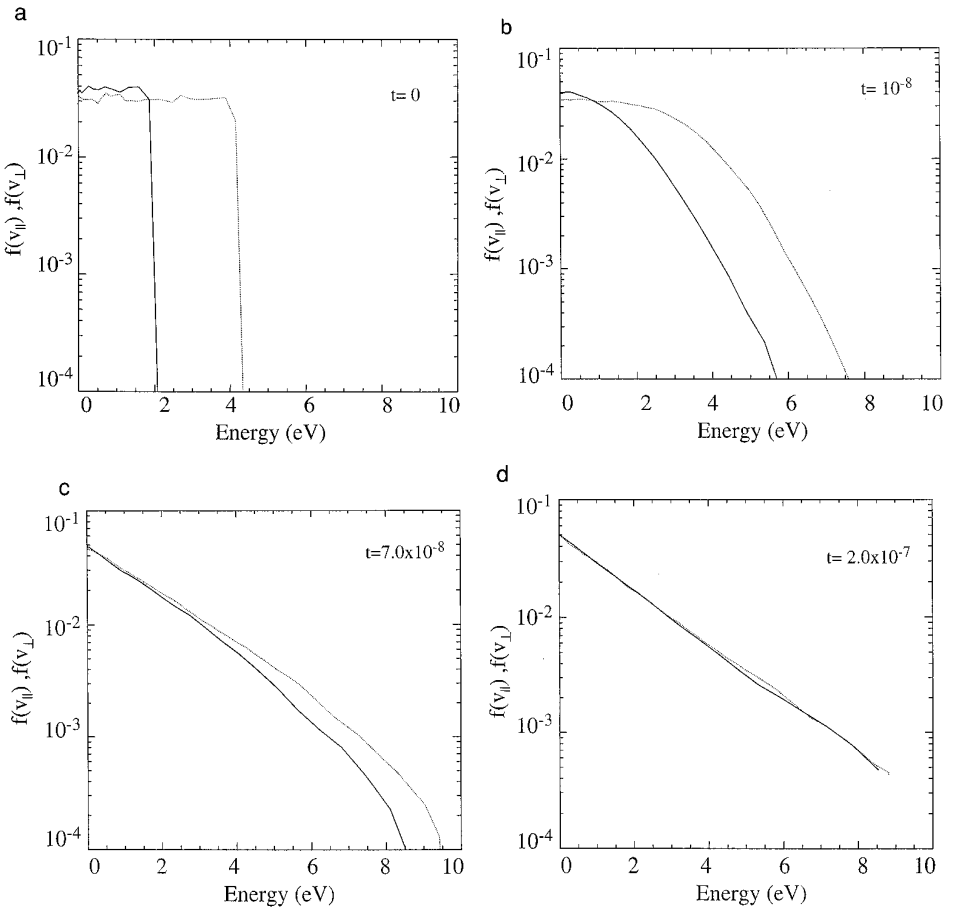

FIG. 3. Reduced electron distribution functions $f(v_\parallel)$ (solid curve) and $f(v_\perp)$ (dashed curve) at times (a) $t = 0$, (b) 1×10^{-8} sec, (c) 7×10^{-8} sec, (d) 2×10^{-7} sec.

and close to Maxwellian in the thermal range, but the high-energy range is still anisotropic and non-Maxwellian. Finally, in Fig. 3d at time 2×10^{-7} sec, the distribution functions are isotropic and Maxwellian over their entire energy range.

B. *Balance Between Heating, e-e Collisions, and Inelastic Collisions*

When the electron distribution function is determined by a competition between different collisional processes, it is obviously important to use a collision formulation which correctly represents the energy dependence of the collision frequencies. In this example we model, in a very simplified way, the combined effect of several processes that occur in an ECR discharge: plasma heating, electron–electron collisions, and electron energy loss due to ionizing collisions. In the model, electrons with energy $\varepsilon < 3$ eV are heated every time they pass a "resonant zone." The heating is implemented by giving each electron a velocity kick each time it passes by the position $z = 3$ cm, with the velocity increment Δv chosen randomly from a

Gaussian distribution with mean value $\frac{1}{2}m(\Delta v)^2 = 1$ eV. We also include electron energy loss due to "ionizing collisions" with neutral atoms. (However, we do not create new electrons when one of these "ionizing collisions" occurs. Since we are simulating a closed system with no particle losses, this would preclude the attainment of steady state.) The ionization cross section for Ar is used, as given by Tachibana [29]. This cross section increases from about 10^{-16} cm^2 just above the ionization threshold $\varepsilon_{iz} = 15.76$ eV, to a maximum of 3.9×10^{-16} cm^2 at 60 eV. Each electron loses exactly 15.76 eV of energy when it is scattered. Electron-impact excitation collisions are omitted from this simple model, even though they do represent a significant energy loss mechanism in a real gas.

We run the simulation until the electron energy distribution function (EEDF) reaches equilibrium. Figure 4 shows the results for several cases with differing values of the plasma density n_e, but with neutral gas pressure equal to 5 mTorr in each case. The e-e collision rate is thus proportional to n_e, while the electron-neutral collision rate is the same for each case. In Fig. 4a, the plasma density is 10^{10} cm^{-3}. As this value of n_e, electron–electron scattering is weak, and ionization energy losses deplete the tail of the distribution function for energies above ε_{iz}. Figure 4b shows the EEDF for a plasma of density 10^{11} cm^{-3}. Here, e-e scattering is strong enough to drive the electron distribution to Maxwellian in the regime below ε_{iz} and to significantly replenish the distribution above the ionization threshold. Figure 4c shows the EEDF for plasma density 10^{12} cm^{-3}. In this case, e-e scattering is easily strong enough to redistribute energy from the heating region $\varepsilon < 5$ eV to the tail region, and the equilibrium distribution is very nearly Maxwellian over the entire energy range.

7. CONCLUSIONS

The Langevin equation can be used to formulate electron–electron and electron–ion collisions in a probabilistic manner analogous to the Monte Carlo treatment that is often applied to electron–neutral or neutral–neutral scattering. The difference is that e-e and e-i collisions are very frequent and very weak, so that the Langevin equation represents the net probabilistic effect of very many small-angle scatterings. Therefore, time steps can be long compared to the time scale for interactions between particular pairs of charged particles. The exact form of the Langevin equation is well known, but is impractical for numerical applications, due to the need for very large numbers of simulation particles, extensive data structures, and burdensome computations. We have used several simple and well-justified approximations to reduce the formulation to a manageable and efficient form, which is accurate when the electron velocity distribution is fairly close to isotropy in the local rest frame of the electrons. If the velocity distribution is highly anisotropic and multi-peaked, e.g., for multiple beams, an accurate treatment of scattering can be done simply by representing the electrons as a superposition of several isotropic distributions displaced from each other in velocity space. We have also provided simple procedures for ensuring that momentum and energy are conserved in the numerical implementation. The general formulation is applicable to either unmag-

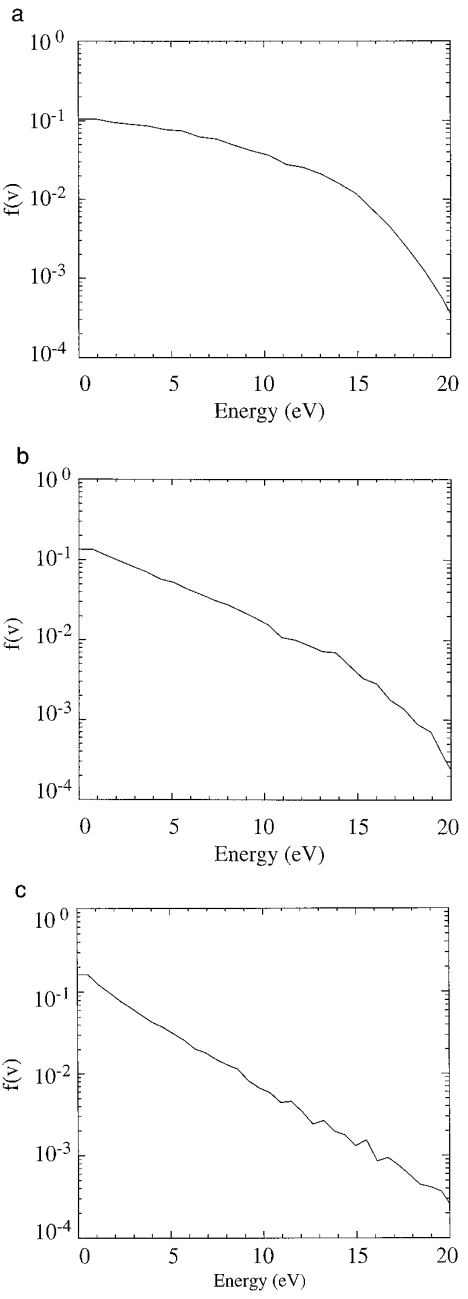

FIG. 4. Electron energy distribution functions for Ar at pressure 5 mTorr, after steady state has been reached. Included are a simple model of bulk electron heating, e-e collisions, and electron energy losses due to ionizing collisions. Excitations, and electron creation and loss are not included. (a) $n_e = 10^{10}$ cm^{-3}; (b) $n_e = 10^{11}$ cm^{-3}; (c) $n_e = 10^{12}$ cm^{-3}.

netized or magnetized electrons, and in the latter case we have expressed the results specifically in terms of the velocity components parallel and perpendicular to **B**.

APPENDIX

In this section we consider the range of validity of the isotropic scatterer assumption made in Section 2B. As a test case, we consider an electron velocity distribution which is a superposition of two displaced Maxwellians,

$$f(\mathbf{v}) = \frac{1}{2}\left(\frac{m}{2\pi T}\right)^{3/2}\left[\exp\left(-\frac{(\mathbf{v}-\mathbf{v}_0)^2}{2v_e^2}\right) + \exp\left(-\frac{(\mathbf{v}+\mathbf{v}_0)^2}{2v_e^2}\right)\right], \tag{A1}$$

where $v_e = (T/m)^{1/2}$ is the electron thermal velocity. This distribution can be varied from isotropic ($\mathbf{v}_0 = 0$) to a completely anisotropic two-beam situation ($v_0 \gg v_e$). Since (A1) is the sum of two distributions each of which is isotropic in its own frame of reference, the exact values of $\mathbf{F}_d$ and $\mathbf{D}$ can be evaluated analytically, as vector or tensor sums of the expressions arising from each term of (A1) and Eqs. (15). We shall consider $\mathbf{F}_d$ as an example. Defining dimensionless velocities $\mathbf{V} \equiv \mathbf{v}/\sqrt{2}v_e$ and $\mathbf{V}_0 \equiv \mathbf{v}_0/\sqrt{2}v_e$, we find

$$\mathbf{F}_d(\mathbf{v}) = -\frac{4\pi^{1/2}ne^4\lambda}{mT}\frac{\mathbf{v}}{v}\left[\frac{\mathbf{V}-\mathbf{V}_0}{|\mathbf{V}-\mathbf{V}_0|^3}\left(\frac{\pi^{1/2}}{2}\operatorname{erf}(|\mathbf{V}-\mathbf{V}_0|) - |\mathbf{V}-\mathbf{V}_0|e^{-|\mathbf{V}-\mathbf{V}_0|^2}\right)\right.$$
$$\left. + \frac{\mathbf{V}+\mathbf{V}_0}{|\mathbf{V}+\mathbf{V}_0|^3}\left(\frac{\pi^{1/2}}{2}\operatorname{erf}(|\mathbf{V}+\mathbf{V}_0|) - |\mathbf{V}+\mathbf{V}_0|e^{-|\mathbf{V}+\mathbf{V}_0|^2}\right)\right]. \tag{A2}$$

Writing $\mathbf{V} = (V_\parallel, V_\perp)$, where $\parallel$ and $\perp$ refer here to parallel and perpendicular to $\mathbf{v}_0$, we consider cases in which $\mathbf{V}$ is on each of the two principal axes of Eq. (A1):

$$\mathbf{F}_d(V_\parallel, 0) = -\frac{4\pi^{1/2}ne^4\lambda}{mT}\frac{\mathbf{v}}{v}\left[\frac{\pi^{1/2}}{2}\frac{1}{(V_\parallel - V_0)^2}\operatorname{erf}(V_\parallel - V_0) + \frac{\pi^{1/2}}{2}\frac{1}{(V_\parallel + V_0)^2}\operatorname{erf}(V_\parallel + V_0)\right.$$
$$\left. - \frac{1}{V_\parallel - V_0}e^{-(V_\parallel - V_0)^2} - \frac{1}{V_\parallel + V_0}e^{-(V_\parallel + V_0)^2}\right], \tag{A3a}$$

$$\mathbf{F}_d(0, V_\perp) = -\frac{8\pi^{1/2}ne^4\lambda}{mT}\frac{\mathbf{v}}{v}\frac{V}{(V^2 + V_0^2)^{3/2}}\left[\frac{\pi^{1/2}}{2}\operatorname{erf}(\sqrt{V^2 + V_0^2}) - (V^2 + V_0^2)^{1/2}e^{-(V^2+V_0^2)}\right]. \tag{A3b}$$

The exact expressions for the dynamical friction from Eqs. (A3) can be compared to the results of the isotropic model of Section 2B. The angular-averaged distribution function, from Eqs. (13) and (A1), is

$$\bar{f}(V) = \frac{1}{4\sqrt{2\pi}v_e^3}\frac{1}{V_0}\left(e^{-(V-V_0)^2} - e^{-(V+V_0)^2}\right). \tag{A4}$$

Using Eq. (A4) in (15a), we find that the dynamical friction according to the isotropic model is

$$\mathbf{F}_d^{iso}(\mathbf{v}) = -\frac{2\pi^{1/2}ne^4\lambda}{mT}\frac{\mathbf{v}}{v}\frac{1}{V^2}\left[\pi^{1/2}\,\mathrm{erf}(V_0+V) - \pi^{1/2}\,\mathrm{erf}(V_0-V) + \frac{1}{V_0}\left(e^{-(V_0+V)^2} - e^{-(V_0-V)^2}\right)\right]. \tag{A5}$$

In Fig. 5, the exact results for $\mathbf{F}_d$ from Eqs. (A3), and the isotropic model result from Eq. (A5), are plotted as a function of V and V_0. We see that the isotropic model is quantitatively accurate (~10% accuracy for all electron velocities) if $V_0 \leq 0.3$, which corresponds to a ratio of parallel to perpendicular temperature $T_\parallel/T_\perp = 1.4$, and is still reasonably accurate (~20% error at worst, and considerably less for most velocities) when $V_0 = 0.5$, i.e., $T_\parallel/T_\perp = 2$. When $V_0 = 0.7$, i.e., $T_\parallel/T_\perp = 3$, the isotropic model begins to differ significantly from the exact $\mathbf{F}_d$ for electrons with $V_\perp < V_\parallel < V_0$. This inaccuracy occurs because at $V_0 = 0.7$, the distribution (A1) is not merely anisotropic, but is actually beginning to be two-peaked. Since Coulomb scattering is strongest between electrons with small relative velocity, the dynamical friction tends to draw an electron toward the closer of the two peaks, rather than toward $\mathbf{v} = 0$. As a result, when V_0 is larger than 0.7, $\mathbf{F}_d$ begins to have a dip for electrons with $V_\perp < V_\parallel < V_0$. For still larger values of V_0, $\mathbf{F}_d$ can actually become negative for these electrons. These features are not reproduced in the isotropic model.

However, this example probably gives a worst case scenario for the accuracy of the isotropic model. To a large extent, the peculiarity of $\mathbf{F}_d$ noted above is canceled out by the effect of the diffusion tensor: both the exact formulation and the isotropic model cause the distribution to evolve toward a single isotropic Maxwellian, even if $\mathbf{F}_d$ is negative at $\mathbf{v} = 0$. If the velocity distribution is anisotropic but not multiply peaked, the isotropic model should give a considerably better representation of $\mathbf{F}_d$ than is the case for the distribution of Eq. (A1). Thus one may expect the isotropic approximation to provide a reasonable representation for anisotropic single-peaked distributions at least to temperature anisotropy somewhat greater than 2. For multi-peaked distributions, i.e., multiple beams, the friction and diffusion coefficients can always be calculated as the vector or tensor sum of contributions from several isotropic distributions displaced from each other in velocity space.

ACKNOWLEDGMENT

The authors appreciate helpful interactions with Dr. Richard F. Femsler and Dr. Steven P. Slinker.

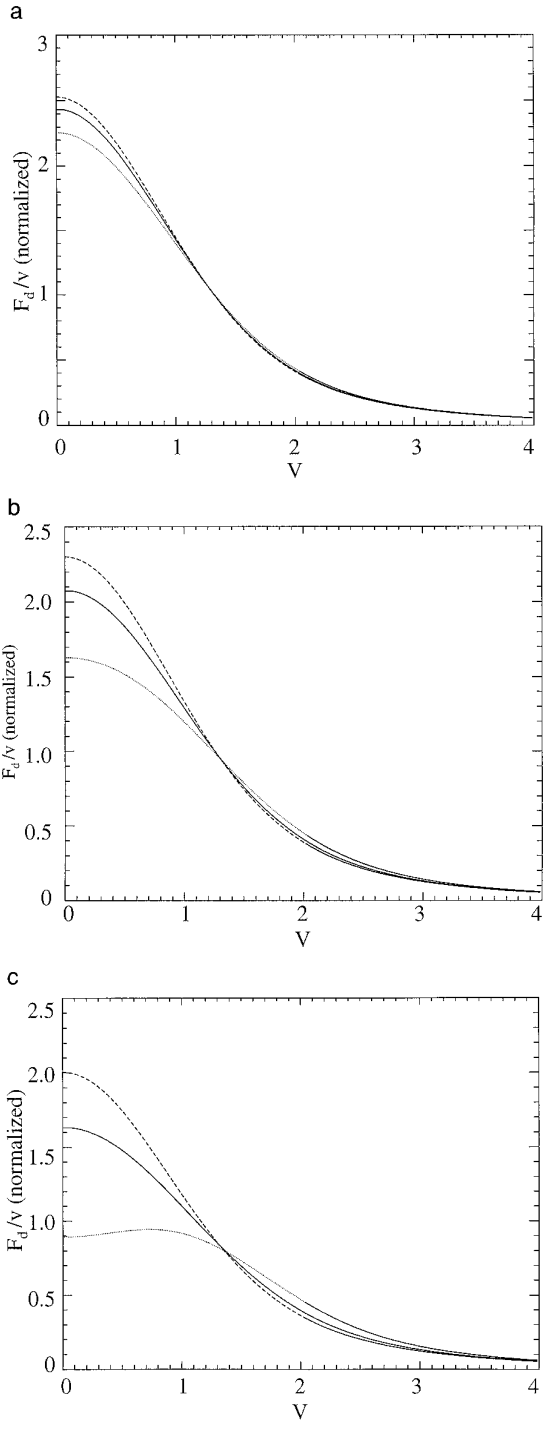

FIG. 5. $F_d^{iso}(v)$ (solid curve), $F_d(V_\parallel, 0)$ (dotted curve), and $F_d(0, V_\perp)$ (dashed curve), for displaced Maxwellian distribution with normalized displacement (a) $V_0 = 0.3$, (b) $V_0 = 0.5$, (c) $V_0 = 0.7$.

REFERENCES

1. C. K. Birdsall and A. B. Langdon, *Plasma Physics via Computer Simulation* (Hilger, Bristol, Philadelphia/New York, 1991).
2. R. W. Hockney and J. W. Eastwood, *Computer Simulation Using Particles* (Hilger, Bristol/New York, 1988).
3. T. Tajima, *Computational Plasma Physics* (Addison–Wesley, Reading, MA, 1989).
4. C. K. Birdsall, *IEEE Trans. Plasma Sci.* **19,** 65 (1991).
5. R. W. Boswell and I. J. Morey, *Appl. Phys. Lett.* **52,** 21 (1988).
6. D. Vender and R. W. Boswell, *IEEE Trans. Plasma Sci.* **18,** 725 (1990).
7. M. Surendra, D. B. Graves, and I. J. Morey, *Appl. Phys. Lett.* **56,** 1022 (1990).
8. R. K. Porteus and D. B. Graves, *IEEE Trans. Plasma Sci.* **19,** 204 (1991).
9. D. B. Graves, H. Wu, and R. K. Porteus, *Japan. J. Appl. Phys.* **32,** 2999 (1993).
10. V. P. Gopinath and T. A. Grotjohn, *IEEE Trans. Plasma Sci.* **23,** 602 (1995).
11. V. Vahedi, C. K. Birdsall, M. A. Lieberman, G. DiPeso, and T. D. Rognlien, *Plasma Sources Sci. Tech.* **2,** 261 (1993).
12. M. M. Turner and M. B. Hopkins, *Phys. Rev. Lett.* **69,** 3511 (1992).
13. K. A. Ashtiani, J. L. Shohet, W. N. G. Hitchon, G.-H. Kim, and N. Hershkowitz, *J. Appl. Phys.* **78,** 2270 (1995).
14. G. A. Bird, *Molecular Gas Dynamics and the Direct Simulation of Gas Flows* (Clarendon, Oxford, 1994).
15. M. Lampe, G. Joyce, W. M. Manheimer, and S. P. Slinker, *Quasineutral Particle Simulation of Magnetized Plasma Discharges: General Formulation and Application to ECR Discharges,* NRL Memorandum Report 6709-97-7960, 1997, in press.
16. M. Lampe, G. Joyce, W. M. Manheimer, and S. P. Slinker, *IEEE Trans. Plasma Sci.*, accepted for publication.
17. M. Lampe, G. Joyce, and W. M. Manheimer, in *Lectures in Plasma Physics and Technology,* edited by V. Stefan (Inst. for Adv. Physics Studies Press, La Jolla, 1997).
18. Y. Weng and M. J. Kushner, *Phys. Rev. A* **42,** 6192 (1990).
19. M. N. Rosenbluth, W. M. MacDonald, and D. L. Judd, *Phys. Rev.* **107,** 1 (1957).
20. D. C. Montgomery and D. A. Tidman, *Plasma Kinetic Theory* (McGraw–Hill, New York, 1964), pp. 15–24.
21. N. A. Krall and A. W. Trivelpiece, *Principles of Plasma Physics* (McGraw–Hill, New York, 1973), Chap. 6.
22. R. J. Procassini and B. I. Cohen, *J. Comput. Phys.* **102,** 39 (1992).
23. A. M. Dimits and B. I. Cohen, *Phys. Rev. E* **49,** 709 (1994).
24. S. Chandrasekhar, *Rev. Mod. Phys.* **15,** 1 (1943).
25. M. E. Jones, D. S. Lemons, R. J. Mason, V. A. Thomas, and D. Winske, *J. Comput. Phys.* **123,** 169 (1996).
26. S. Chandrasekhar, *Astrophys. J.* **97,** 255 (1943).
27. T. G. Northrop and T. J. Birmingham, *Planet. Space Sci.* **38,** 319 (1990).
28. D. S. Lemons, J. Lackman, M. E. Jones, and D. Winske, *Phys. Rev. E* **52,** 6855 (1995).
29. K. Tachibana, *Phys. Rev. A* **34,** 1007 (1986).